Modal synthesis and dynamical condensation methods for accurate piezoelectric systems impedance computation

Manuel Collet, K.A. Cunefare

Modal Synthesis and Dynamical Condensation Methods for Accurate Piezoelectric Systems Impedance Computation

M. COLLET[1,*] AND K. A. CUNEFARE[2]

[1]*FEMTO-ST, Dept Applied Mechanics: UMR-CNRS 6174, and International Joint Research Unit: UMI2958 Georgia Tech-CNRS, 24 Chemin de l'Epitaphe, 25000 Besancon, France*

[2]*G.W Woodruff School of Mechanical Engineering, 113 Erskine Love Building, Atlanta, GA 30332-0405, USA*

ABSTRACT: This article proposes a new, simple and efficient approach, allowing one to reduce and construct piezoelectric super elements guaranteeing an accurate representation of the electrical impedance without the need for static correction. This allows the electronic coupling to be fully addressed in the optimization of passive shunted piezoelectric transducers, energy harvesting piezoelectric systems or dense distributed transducers. The model obtained through this approach is also versatile, of small size, and is therefore quite tractable for use in intensive computation algorithms. Two example systems are used to demonstrate the numerical accuracy and convergence properties of the proposed approach.

Key Words: piezoelectric modeling, substructuring, model condensation, electric impedance.

INTRODUCTION

Nowodays, piezoelectric transducers are widely used in many physical and industrial applications.
Optimization of their behavior is of major interest to extend their capability for sensing and actuating mechanical systems. In current practice, smart structure integration involves a broad multiphysical modeling approach including mechanics, smart materials, coupling effects and electronics implementation. When global energy optimization is considered, all coupling mechanisms should be carefully introduced in the simplest possible modeling procedure. For piezoelectric material these constraints involve the construction of a robust model (simple and precise) able to represent the piezoelectric coupling, or from another perspective, to correctly implement piezoelectric electromechanical impedances. This latter perspective enables the optimization and design of electronic devices connected to the piezoelectric material. Implementation of such an approach is based on the use of a representative piezoelectric finite element model but also on a dedicated model condensation procedure able to reduce the size of the resulting system of equations. The objective of this article is to develop and demonstrate a model reduction approach that yields a piezoelectric super element guaranteeing accurate computation of a piezoelectric transducer's mechanically coupled electrical impedance.

Since the early 1970s, many finite element models have been proposed for analysis of piezoelectric mechanical systems. The survey article of Benjeddou (2000), and the articles by Noor (1991) and Mackerle (1997) discuss a wide variety of different works in this area. After numerous publications devoted to ultrasonic transducers through the early 1990s (Allik, 1970; Allik, 1974), the majority of work for the last two decades has been dedicated to the development of a variety of piezoelectric finite elements for sandwich beams (Collet and Walter, 2003, Maurini, 2004), plates (Lee, 1989a; Banks and Smith, 1996; Ha, 1990; Kogl, 2005; Lee, 1990; Lee and Chiang, 1991; Wang, 2004; Fernadez, 2004; Tzou, 1994a; Tzou1, 1997; Saravanos and Heyliger, 1997), layered composite shells (Yang and Saigal, 1996; Kogl, 2005; Bernadou, 2003; Banks and Smith, 1996) or volume elements like those used in many finite element codes (Lin and Abatan, 1994; Varadan and Lim, 1996; Tzou1, 1997). In fact, finite element method applications are rapidly growing and many works already address the development and implementation of new piezoelectric finite element tools for linear and nonlinear analysis. The advantages and disadvantages of each approach are not discussed here, but we can state that, today, most of the physical applications can be more or less precisely modeled using existing methods.

As noted in (Benjeddou, 2000), the most theoretically advanced finite elements has not been widely used for practical modeling of adaptive structural elements for 'intelligent' or smart materials and

*Author to whom correspondence should be addressed.
E-mail: manuel.collet@univ-fcomte.fr

structures applications. Because of the difficulty in building accurate and reduced models for multiphysics analysis, many authors have used simplified modeling approaches in order to limit numerical complexity while focusing on the physical design, computation and optimization (Hagood, 1991; Crawley, 1994; Rao, 1994; Preumont, 1997; Collet and Walter, 2003; Monnier, 2005). This particular area of interest drives the simplifications applied to the modeling. Indeed, introducing full modeling of the electromechanical coupling leads to the use of extended three-dimensional finite element formulations containing both electric and mechanical degree of freedoms (DOFs). Also, considering the electric contribution in the discretization procedure is a difficult task, especially for conventional one- or two-dimensional mid-plane formulations. The most common assumption is to consider through-thickness linear variation of the electrical potential (Lee, 1989a; Lee, 1989b; Lee, 1990; Hagood, 1991; Lee and Chiang, 1991; Hac, 1993; Tzou, 1994b; Preumont, 1997; Collet and Walter, 2003). This hypothesis leads to neglecting the induced potential while the electromechanical coupling will be only partially captured as described in (Benjeddou, 2000). This approach can yield up to 30% error in evaluating the equivalent piezoelectric capacity for small patches. In fact, it is known that the asymptotic electric potential for a short-circuited thin plate is quadratic in the thickness (Rajapakse, 1997; Bernadou, 2003).

The current challenge in designing efficient and integrated smart systems for active and passive control or energy harvesting leads to the use of large multiphysical models including accurate representation of electromechanical couplings. The growing attention to smart distributed structures (Vidoli, 2001) and MEMS piezoelectric systems (Collet and Delobelle, 2004; Meyer and Verdot, 2007) requires new modeling approaches guaranteeing robust representation of electromechanical coupling, especially for piezoelectricity. This will enable the introduction of electronic devices directly in the design and optimization process and lead to the development of new efficient and robust systems. At present, the only way to achieve this modeling goal is to use higher order 2D-theory for plates or shells (Carrera, 1997; Chattopadhyay, 1997; Bernadou, 2003; Fernadez, 2004; Maurini and dell'Isola, 2004) or full 3D bricks (Lin and Abatan, 1994; Varadan and Lim, 1996; Tzou, 1997). The principal problem with such an approach is the numerical complexity of the finite element formulation and the size of the resulting algebraic system of equations. Classical Guyan condensation of the electrical DOFs can be used. This leads to an increase of the structure's stiffness and an additional load vector that is difficult to manage when construction of super elements is considered (super elements are equivalent models with greatly reduced numerical DOFs as compared to fully meshed models). Direct projection of the new external load onto the reduced basis as in (Becker and Fein, 2006) allows one to conserve the actuating effect in the super element construction but then needs to be corrected for each specific use by static response computations for accurate representation of electrical impedance as for mechanical modal synthesis of the final assembled system (Geradin, 1997). Guyan or Craig and Bampton methods could also be used by adding applied voltage as a master DOF but leads to introduced inertial coupling and the need for knowledge of its second time derivative.

This article proposes a new, simple, and efficient approach, allowing one to reduce and construct piezoelectric super elements guaranteeing an accurate representation of the electrical impedance without the need for static correction. This allows the electronic coupling to be fully used in the optimization of passive shunted piezoelectric transducers, energy harvesting piezoelectric systems or dense distributed transducers. The obtained model through this approach is also versatile, of small size, and is therefore quite tractable for use in intensive computation algorithms.

The article is organized as follows. The first section presents the theoretical models for piezoelectric systems. The next section introduces the numerical procedure leading to model reduction and super element construction. Thereafter, two examples are considered to validate the proposed method. The first example is that of a full condensation of a piezoelectric stack transducer. The second example is that of a piezoelectric composite plate modeled using an extended full 3D approach. Concluding remarks end the article.

LINEAR PIEZOELECTRIC MECHANICAL SYSTEMS MODELING AND CONDENSATION

Theoretical Model Synthesis for Substructuring Approach

Consider the generic piezo-mechanical system as depicted in Figure 1. It represents a mechanical structure on an open domain Ω of $\mathbb{R}^3$ and its general boundary conditions applied to a partition of its surface S so that $S = S_u \cup S_\sigma$ where S_u denotes the location of Dirichlet boundary conditions and S_σ those of Neumann boundary conditions. f represents the exterior forces and w the displacement vector. A set of piezoelectric transducers is connected to this mechanical system. The inputs are P applied voltages V_p on a partition of the piezoelectric domain's boundaries S^u_{vq}. The outputs are the corresponding dual charge q_p. The piezo-mechanical transducer system is precisely shown in Figure 2, where Ω_p represents the piezoelectric domain, and Ω_s represents the structural domain consisting of the connections of each transducer. The boundary surfaces are partitioned

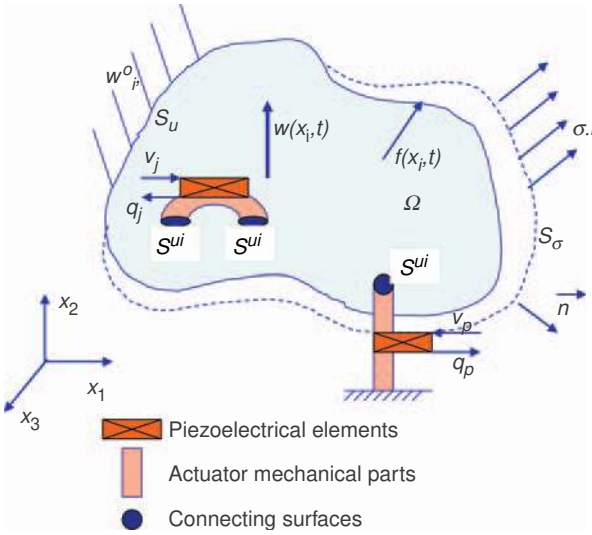

Figure 1. *General piezomechanical system description.*

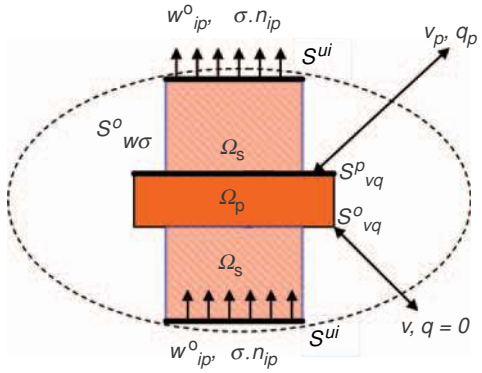

Figure 2. *General piezoelectric transducer system description.*

such that S^{u_i} represents the connecting interfaces, $S^o_{w\sigma}$ the localization of the homogeneous Neumann or Dirichlet mechanical boundary conditions, S^p_{vq} the inputs/outputs electrical surfaces and S^o_{vq} the homogeneous Neumann and Dirichlet electrical boundary conditions.

The classical 3D electromechanical dynamical equilibrium can be written as

$$\begin{cases} \rho\ddot{w} - \nabla\sigma = f & \forall x \in \Omega \cup \Omega_p \\ -\nabla D = 0 & \forall x \in \Omega_p \end{cases} \tag{1}$$

with associated mechanical boundary conditions

$$\begin{cases} w = w_o & \forall x \in S_u \cup S^o_w \\ \sigma \cdot n = T_o & \forall x \in S_\sigma \cup S^o_\sigma \\ [w] = [\sigma \cdot n] = 0 & \forall x \in \bigcup_{i\in[1..I]} S^{u_i} \end{cases} \tag{2}$$

and electrical boundary conditions

$$\begin{cases} V = 0 & \forall x \in S^o_v \\ V = V_p & \forall x \in \bigcup_{p\in[1..P]} S^p_{vq} \\ D \cdot n = 0 & \forall x \in S^o_q \end{cases} \tag{3}$$

In the above equations [] represents the jump value, I stands for the number of interfaces between each transducer and the main structure and P is the number of piezoelectric input voltages. We add to this set of equilibrium equations an output expression

$$q_p = -\int_{S^p_{vq}} D_n dS \; p \in [1..P] \tag{4}$$

allowing the introduction of the charge measurement and hence the dual counterpart of the imposed electrical Dirichlet boundary condition.

For the sake of simplicity we consider, in the following, only homogeneous mechanical Dirichlet boundary conditions such as $w_o = 0$. The linear constitutive material behavior relationships can be written as

$$\sigma = c_E(x)\epsilon - e^T(x)E \tag{5}$$

$$D = e(x)\epsilon + \varepsilon_S(x)E \tag{6}$$

where σ represents the Cauchy stress tensor, $\varepsilon = \nabla_{sym} w$ the Green strain tensor, $E = -\nabla V$ the electric field vector (V the voltage), C_E the elasticity tensor at constant electrical field, e^T the piezoelectric coupling tensor and ε_S the dielectric permittivity at constant strain.

The equations above are consistent for each kind of material to the extent that null piezoelectric and permittivity tensors can be used when passive materials are considered. All of these tensors also depend on the spatial location vector x.

For arbitrary admissible virtual mechanical displacements δw and voltage δV, by introducing the Lagrange multipliers T_{u_i}, δq_p, and δq_o associated, respectively with the nonhomogeneous Dirichlet boundary conditions rewritten in Equations (8) and (9), Equations (1), (2), and (3) are equivalent to Equation (7).

$$\begin{aligned} &\int_{\Omega\cup\Omega_p} (\nabla\sigma + f - \rho\ddot{w}) \cdot \delta w d\Omega + \int_{\Omega_p} \nabla D \delta V d\Omega \\ &+ \int_{\bigcup_{i\in[1..I]} S^{u_i}} [w]\delta T_{u_i} d\Gamma + \int_{\bigcup_{p\in[1..P]} S^p_{vq}} (V - V_p)\delta q_p d\Gamma \\ &+ \int_{S^o_v} v\delta q_o d\Gamma + \int_{S_u\cup S^o_w} (w - w_o)\delta T_w d\Gamma = 0 \end{aligned} \tag{7}$$

$$w_s - w = 0 \; \forall x \in \bigcup_{i\in[1..I]} S^{u_i}_{w\sigma} \tag{8}$$

$$V = V_p \; \forall x \in \bigcup_{p\in[1..P]} S^p_{vq}. \tag{9}$$

By integrating by parts, splitting w into its components on the main structure w_s and those on the piezoelectric transducers w, and introducing the Neumann conditions of Equations (2) and (3) as well as the constitutive Equations (5), (6), we formally obtain the variational formulation of our continuous problem as follows:

For all δw_s, δw, δV virtual mechanical displacement piezoelectric displacements and voltage in a suitable admissible space and δT_{u_i} and δq_p Lagrange multipliers

associated with nonhomogeneous Dirichlet conditions, the partial derivative problem in Equations (1–3) is equivalent to :

$$\begin{aligned}
&\int_{\Omega} \rho\ddot{w}\delta w_s + c\nabla_{\mathrm{sym}} w_s \nabla_{\mathrm{sym}}\delta w_s - f\delta w_s d\Omega \\
&+ \int_{\Omega_p} \rho\frac{\partial^2 w}{\partial t^2}\delta w + c_E\nabla_{\mathrm{sym}} w\nabla_{\mathrm{sym}}\delta w + e^T\nabla V\nabla_{\mathrm{sym}}\delta w - f\delta w d\Omega \\
&+ \int_{\Omega_p} -e\nabla_{\mathrm{sym}} w\nabla\delta V + \varepsilon\nabla V\nabla\delta V d\Omega \\
&- \int_{S_\sigma} T_o\delta w_s d\Gamma - \int_{\bigcup_{i\in[1..I]} S^{u_i}} T_{u_i}\delta w_s d\Gamma \\
&- \int_{S^o_\sigma} T_o\delta w d\Gamma - \int_{\bigcup_{i\in[1..I]} S^{u_i}} (-T_{u_i})\delta w d\Gamma \\
&- \int_{\bigcup_{p\in[1..P]} S^p_{vq}} q_p\delta V d\Gamma + \int_{\bigcup_{i\in[1..I]} S^{u_i}} (w_s - w)\delta T_{u_i} d\Gamma \\
&+ \int_{\bigcup_{p\in[1..P]} S^p_{vq}} (V - V_p)\delta q_p d\Gamma = 0. \qquad (10)
\end{aligned}$$

By using the Finite Element discretization technique, we obtain a set of algebraic equations for the structural behavior as

$$\begin{aligned}
&\begin{bmatrix} M^s_{ii} & M^s_{ic} \\ M^{sT}_{ic} & M^s_{cc} \end{bmatrix}\begin{bmatrix} \ddot{w}_{si} \\ \ddot{w}_{sc} \end{bmatrix} + \begin{bmatrix} K^s_{ii} & K^s_{ic} \\ K^{sT}_{ic} & K^s_{cc} \end{bmatrix}\begin{bmatrix} w_{si} \\ w_{sc} \end{bmatrix} \\
&\quad = \begin{bmatrix} f^s + T^s_o \\ \sum_{i\in[1..I]} -T^s_{u_i} \end{bmatrix} \qquad (11) \\
&w_{sc} - w_c = 0
\end{aligned}$$

and for the piezoelectric transducer as

$$\begin{aligned}
&\begin{bmatrix} M_{ii} & M_{ic} & 0 & 0 \\ M^T_{ic} & M_{cc} & 0 & 0 \\ 0 & 0 & 0 & 0 \\ 0 & 0 & 0 & 0 \end{bmatrix}\begin{bmatrix} \ddot{w}_i \\ \ddot{w}_c \\ \ddot{V} \\ \ddot{V}_p \end{bmatrix} \\
&+ \begin{bmatrix} K_{ii} & K_{ic} & E_i & E_{ip} \\ K^T_{ic} & K_{cc} & E_c & E_{cp} \\ -E^T_i & -E^T_c & C & C_p \\ -E^T_{ip} & -E^T_{cp} & C^T_{cp} & C_{pp} \end{bmatrix}\begin{bmatrix} w_i \\ w_c \\ V \\ V_p \end{bmatrix} = \begin{bmatrix} f + T_o \\ \sum_{i\in[1..I]} T^s_{u_i} \\ 0 \\ Q_p \end{bmatrix}. \qquad (12) \\
&w_{sc} - w_c = 0
\end{aligned}$$

For notational simplicity the same variable labels are used for the continuous functions and their discretized counterparts. Each set of equations has been reorganized through introducing sub-vectors of DOFs. In Equation (11), w_{si} is used to denote the internal structural DOFs and w_{sc} those of the connecting surface as they naturally appear in the mechanical part of the term $\int_{\cup_{i\in[1..I]} S^{u_i}} (w_s - w)\delta T_{u_i} d\Gamma$ of the weak formulation in Equation (10). In the same manner, the transducer DOFs are split as w_i for the inner part and w_c for the connecting part of the displacement. Partition of the voltage terms is introduced by using V for unknown voltage DOFs and V_p for the applied piezoelectric potential. The output Equation (4) for each electrode S^p_{vq} is the last line of the matrix in Equation (12).

With respect to the modeling development note the following:

- Homogeneous Dirichlet boundary conditions have been directly removed from the modeling by use of a *suitable admissible* space compatible with these constraints. Of course, the same approach could be used if we need to determine their dual quantities such as the input charges on the ground electrodes S^o_v or the reactive forces on constrained surfaces S^o_w or S_u.
- The variational problem introduced here concerns a 3D modeling of the entire system. Any approach (beam, plate, shell) can be used as far as the model of interest retains the complete piezoelectric coupling effect.
- According to (Benjeddou, 2000) our method permits the consideration of the 'induced electrical potential' and does not introduce any constraint on each surface's charge fields q_p dual to the applied voltages V_p even if it does not explicitly appear in Equation (12), but only through its integral form $Q_p = \sum q_p$.
- The entire piezo-mechanical system could be modeling using one set of Equations through elimination of the interconnecting forces δT_{u_i}.

At this point, we have obtained a coupled system of equations that have to be reduced and solved. The structural part in Equation (11) may be treated using any kind of model condensation method such as Guyan, Craig, and Bampton (Geradin, 1997) or dual FETI (Rixen, 1998). The principal interest of this article, though, is the condensation of the piezoelectric elements, which is addressed in the next section.

The Proposed Piezoelectric Condensation Technique

The proposed condensation method is based on using the static Schur complement (Bernadou, 2003) of the stiffness matrix obtained in Equation (12). This approach has been used in previous work (Varadan and Lim, 1996; Bernadou, 2003; Wang, 2004) to reduce the number of piezoelectric DOFs for large system computation. The following shows how this natural method leads to an original strategy for piezoelectric condensation, allowing an accurate computation of the piezoelectric impedances.

First, consider the Schur complement applied to the piezoelectric set of Equations (12). As Equation (12) indicates, the electrical response behavior of such a system is essentially static. In fact, by simply introducing the Schur complement of the first 3×3 block of the

stiffness matrix K, the dynamical equilibrium of our piezoelectric system is equivalent to

$$\begin{bmatrix} M_{ii} & M_{ic} & 0 \\ M_{ic}^T & M_{cc} & 0 \\ 0 & 0 & 0 \end{bmatrix} \begin{bmatrix} \ddot{w}_i \\ \ddot{w}_c \\ \ddot{V} \end{bmatrix} + \begin{bmatrix} K_{ii} + E_i C^{-1} E_i^T & K_{ic} + E_i C^{-1} E_c^T & 0 \\ K_{ic}^T + E_c C^{-1} E_i^T & K_{cc} + E_c C^{-1} E_c^T & 0 \\ -E_i^T & -E_c^T & C \end{bmatrix} \begin{bmatrix} w_i \\ w_c \\ V \end{bmatrix} = \begin{bmatrix} -E_{ip} + E_i C^{-1} C_p \\ -E_{cp} + E_c C^{-1} C_p \\ -C_p \end{bmatrix} \cdot V_p + \begin{bmatrix} f + T_o \\ \sum_{i \in [1..I]} T_{u_i}^s \\ 0 \end{bmatrix} \quad (13)$$

$$w_{sc} - w_c = 0$$

$$Q_p = (-E_{ip}^T + C_p^T C^{-1} E_i^T) w_i + (-E_{cp}^T + C_p^T C^{-1} E_c^T) w_c + (C_{pp} - C_p^T C^{-1} C_p) V_p. \quad (14)$$

With the C matrix being assumed definite, Equation (12) is equivalent to Equations (13) and (14). Thus we consider w_i, w_c, and V as the state variables of the main equilibrium Equation (13) and the imposed piezoelectric voltages V_p as an input variable.

Also, by introducing the matrix product $\left[\begin{smallmatrix} -C^{-1}C_p \\ I \end{smallmatrix}\right] V_p = \left[\begin{smallmatrix} \bar{V}_p^o \\ I \end{smallmatrix}\right] V_p = V_p^o V_p$ gathering all the static dielectric solutions of

$$\begin{bmatrix} C & C_p \\ C_p^T & C_{pp} \end{bmatrix} \begin{bmatrix} V \\ V_p \end{bmatrix} = \begin{bmatrix} 0 \\ Q_p^o \end{bmatrix} \quad (15)$$

for each different applied voltage and by adopting a simplified bloc matrix notation, Equations (13) and (14) can be rewritten as:

$$M\ddot{w} + (K + EC^{-1}E^T) w = -E_p^o \cdot V_p^o \cdot V_p + F + T$$
$$-E^T \cdot w + C\bar{V} = -\bar{C}_p^o \cdot V_p^o \cdot V_p \quad (16)$$

$$Q_p = -V_p^{oT} E_p^{oT} w + C_p^o V_p \quad (17)$$

where F and T stand for the external disturbing forces and the connection reactions, $\bar{V} = V - \bar{V}_p^o V_p$ is the induced electrical potential, $w = \left[\begin{smallmatrix} w_i \\ w_c \end{smallmatrix}\right]$, $E_p^o = \left[\begin{smallmatrix} E_i & E_{ip} \\ E_c & E_{cp} \end{smallmatrix}\right]$, $E = \left[\begin{smallmatrix} E_i \\ E_c \end{smallmatrix}\right]$, $\bar{C}_p^o = [C \quad C_p]$, and M and K are, respectively, the first 2×2 block of the mass and stiffness matrices in Equation (13). We also introduce the equivalent piezoelectric capacitance (for zero displacement) $C_p^o = C_{pp} - C_p^T C^{-1} C_p$. We emphasize that Equations (16) and (17) are strictly equivalent to Equations (12) and (4) including the induced electric potential in the second equation of (16) and in the terms of equality in Equation (17).

At this point, note that most of the previous works (Lee, 1989a; Lee, 1990; Lee and Chiang, 1991; Hac, 1993; Collet, 1995, 2001; Collet and Walter, 2003), introduce actuation or sensing behavior by considering zero charge or zero electrical field on the electrodes. In our work, we build a reduced order model allowing us to accurately compute the electrical impedance of such a piezoelectric system. As can be seen in Equation (12), the electrical behavior is only 'static' with zero terms in the mass matrix acting on the second time derivative of the voltage. The approach must also take into account this static field and integrate it into the basis used for condensation. Thus, we avoid the use of the classical modal synthesis method that would lead us to add static correcting terms to the electrical output equations. These static terms depending on the global electromechanical system behavior given by the coupled Equations (11) and (12) could not be computed by considering only the sub-structure equilibrium. The direct use of Craig and Bampton methods to condense the piezoelectric coupled system in Equation (12) would introduce a full mass matrix, coupling the electrical voltage DOFs to the other generalized coordinates. Thus, we would need to use a second electrical inputs term $\ddot{V}_p$ which is not intrinsically a desirable approach.

The key novelty of our proposed method is to add the dual static displacement field adjoint to the imposed piezoelectric force $-E_p^o.V_p^o$ in Equation (16) to the original Craig and Bampton basis. Therefore, the proposed approximation basis may be represented as three sets of displacement fields:

1. The classical static Craig and Bampton displacement field corresponding to the static solutions of the unitary nonhomogeneous Dirichlet imposed connecting conditions. These fields are constrained to be orthogonal to the applied piezoelectric force. The solutions $W_u = \left[\left\{\begin{smallmatrix} w_{u_i} \\ V_{u_i} \end{smallmatrix}\right\}_{\forall i}\right]$ are also solutions of the generic mechanical problem

$$\begin{aligned} &(K + EC^{-1}E^T) w_{u_i} = 0 \\ &-E^T \cdot w_{u_i} + C V_{u_i} = 0 \\ &B_u(i,:) w_{u_i} = 1 \\ &-w_{u_i}^T E_p^o V_p^o = 0 \end{aligned} \quad (18)$$

   where B_u represents the localization boolean matrix of the connecting DOFs such as for each i designating a particular connecting DOFs $B_u(i,:)w = w_c(i) = 1$, where $B_u(i,:)$ is the ith row of B_u.
2. A set of the dual displacement fields adjoint to the piezoelectric applied forces computed with homogeneous connecting Dirichlet condition. These displacements $W_{v_p} = \left\{\left[\begin{smallmatrix} w_{v_p} \\ V_{v_p} \end{smallmatrix}\right]\right\}_{\forall p}$ are solutions of the generic mechanical problem

$$\begin{aligned} &(K + EC^{-1}E^T) w_{v_p} = 0 \\ &-E^T w_{v_p} + C V_{v_p} = 0 \\ &B_u w_{v_p} = 0 \\ &-w_{v_p}^T E_p^o V_p^o(:,p) = 1 \end{aligned} \quad (19)$$

   for each p applied unitary static potential vector $V_p^o(:,p)$ ($V_p^o(:,p)$ represents the pth column of the static dielectric solutions matrix V_p^o).

3. A set of fields that are the inner normal modes with homogeneous Dirichlet connecting conditions, orthogonal to the piezoelectric applied forces. These N fields are represented as $\Phi_N = \left[\left\{ \begin{smallmatrix} \phi_n \\ V_{\phi_n} \end{smallmatrix} \right\}_{\forall n}\right]$ and are the first N solutions of the eigenvalue problem represented by

$$\begin{aligned} &(-\omega_n^2 M + (K + EC^{-1}E^T))\phi_n = 0 \\ &-E^T\phi_n + CV_{\phi_n} = 0 \\ &B_u\phi_n = 0 \\ &-\phi_n^T \begin{bmatrix} E & E_p \end{bmatrix} V_p^o = 0. \end{aligned} \tag{20}$$

The number of DOFs in Equations (12) can also be reduced by simply assuming serial truncation as in

$$\begin{bmatrix} w_i \\ w_c \\ V \\ Vp \end{bmatrix} \approx \begin{bmatrix} W_u^{w_i} \\ W_u^{w_c} \\ W_u^V \\ 0 \end{bmatrix} w_c + \begin{bmatrix} W_{v_p}^{w_i} \\ W_{v_p}^{w_c} \\ W_{v_p}^V \\ 0 \end{bmatrix} \eta_p + \begin{bmatrix} \Phi_N^{w_i} \\ \Phi_N^{w_c} \\ \Phi_N^V \\ 0 \end{bmatrix} \eta_n + \begin{bmatrix} 0 \\ 0 \\ \bar{V}_p^o \\ I_p \end{bmatrix} V_p \tag{21}$$

where the notation W^{dof} represents the vector partition corresponding to the DOFs in the superscript.

By using the classical covariant transformation, Equations (12) can be reduced to

$$\begin{aligned} &\begin{bmatrix} M_{cc} & M_{cp} & M_{cn} \\ M_{cp}^T & M_{pp} & M_{pn} \\ M_{cn}^T & M_{pn}^T & I_N \end{bmatrix} \begin{bmatrix} \ddot{w}_c \\ \ddot{\eta}_p \\ \ddot{\eta}_n \end{bmatrix} + \begin{bmatrix} K_{cc} & K_{cp} & 0 \\ K_{cp}^T & K_{pp} & 0 \\ 0 & 0 & \Omega_N^2 \end{bmatrix} \begin{bmatrix} w_c \\ \eta_p \\ \eta_n \end{bmatrix} \\ &= \begin{bmatrix} \sum_{i\in[1..I]} T_{u_i}^s \\ 0 \\ 0 \end{bmatrix} + \begin{bmatrix} 0 \\ I_p \\ 0 \end{bmatrix} \cdot V_p + F + T_o \\ &w_{sc} - w_c = 0 \end{aligned} \tag{22}$$

and

$$q_p = \begin{bmatrix} 0 & I_p & 0 \end{bmatrix} \begin{bmatrix} w_c \\ \eta_p \\ \eta_n \end{bmatrix} + C_p^o V_p \tag{23}$$

where I_N stands for the N order unitary matrix, Ω_N for the diagonal matrix of the eigenvalues ω_n solutions of Equation (19) and F and T are the projection of the exterior applied forces onto the basis.

Remarks

The proposed method is totally compatible with substructuring techniques such as the classical Craig and Bampton approach. The output Equation (23) allows the computation of the piezoelectric impedance of the super element and therefore of the assembled system. Thus, we can use it to describe a piezoelectric transducer's behavior in a complete formulation, integrating the static electrical input/output relationships via the feedthrough term C_p^o and taking into account complete piezoelectric behavior such as the induced potential. The classical approximation orders established for the Craig and Bampton technique hold here, as detailed in (Geradin, 1997).

As previously mentioned, this approach can be used with any kind of piezoelectric modeling for beams, plates, shells or composite structures, even if the electrical behavior does not appear as a standard DOF as it does in (Lee, 1989a; Lee, 1990; Lee and Chiang, 1991; Hac, 1993) for composite beams and plates.

SUBSTRUCTURED MODELING OF A PIEZOSTACK TRANSDUCER CONNECTED TO A BEAM

System Overview

The structure of interest is depicted in Figure 3. It is a 2D plane stress state model of a beam element (substructure 2) connected to an active substructure containing a piezostack transducer. The ends of the beam are assumed to be clamped. The main aim of our computation is to furnish an accurate piezoelectric super element of the active substructure by using the methodology developed above. The final assembled system should exhibit the same static and dynamic behavior as a directly meshed structure and therefore the same impedance.

THE ACTIVE SUBSTRUCTURE

The active substructure (substructure 1 in Figure 3) is more precisely depicted in Figure 4. The mechanical characteristics of the steel beam are presented in Table 1, while those of the piezostack are in Table 2.

The mechanical boundary conditions indicated in Figure 4 are clamped on the left end and

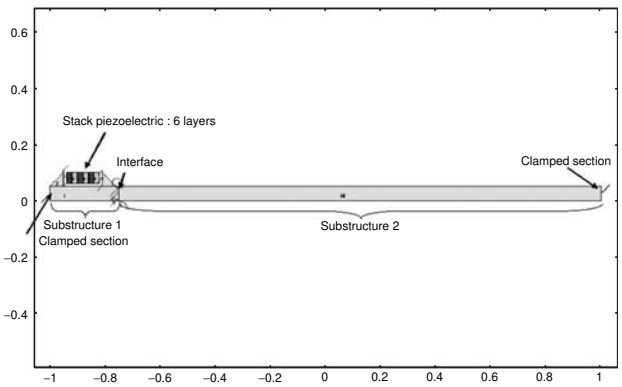

Figure 3. *Mechanical system overview, indicating substructuring between piezoelectric section and passive section.*

'Bernoulli Euler' kinematic fields on the right-hand interface. On this right-hand interface, the 2D displacements $u_i(y,t)$ and $w_i(y,t)$, respectively along axis Ox and Oy, are

$$u_i(y,t) = u_i^o(t) - \left(y - \frac{l_r}{2}\right)\theta_i^o(t) \tag{24}$$

$$w_i(y,t) = w_i^o(t) \tag{25}$$

where l_r represents the section height.

The electrical boundary conditions are also depicted in Figure 4. The lateral edges of each stack layer are free of electrical charge. The connecting stack interfaces are alternatively grounded and subjected to an applied common electrical potential V_p. The piezostack component is connected to the support at the center of its left- and right-hand face to simulate a ball joint.

The initial mesh has 1312 Lagrange-Quadratic triangle elements with four Gauss points per element. The initial total number of DOFs to mesh this part is 7182.

Remarks on numerical implementation:

- Comsol © Multiphysic software is used for implementing the model. The necessary implementation of nonclassical Dirichlet constrains, as in Equations (18–20), may be directly introduced using this software platform. The details are omitted here, but note that the piezoelectric dual constraint is introduced as a sub-domain integral constraint. Integrations are carried out in each piezoelectric sub-domain by using an electro-static field V_p^o (here $p = 1$) obtained by solving Equation (15), as indicated by

$$\text{DualConst} = \int_{\Omega_p} -e^T \nabla V_p^o \nabla_{\text{sym}} \delta w d\Omega. \tag{26}$$

  These general constraints are also set to be equal to 0 in Equation (18) and (20) or equal to 1 in Equation (19).
- Other classical constraints are directly imposed by using coupling variables assigned to be constant. Such is the case for the 'Euler Bernoulli' connective displacement constraints.
- It must be emphasized, in the case of the global computation of response involving Neumann electrical constraints (electrical charge applied to the electrodes), the dual voltage is set to be identical on all the participating electrode surfaces in order to enforce infinite current conductivity on the electrode. Obviously, additional partial derivative Equations can be implemented if one seeks to consider resistance behavior.

Table 1. Steel characteristics.

Structural Steel		
Name	**Values**	**Mechanical properties**
E	200.10^9 Pa	Young Modulus
ν	0.28	Poisson Ratio
ρ	7800 kgm^{-3}	Density
la_r	0.01 m	width
l_r	0.05 m	height

THE PASSIVE BEAM

The mechanical characteristics of the supporting steel beam are presented in Table 1. The boundary conditions described in Figure 5 are clamped on the right end section and 'Euler Bernoulli' kinematic fields on the interface section as indicated in Equations (24) and (25). The initial mesh has 416 Lagrange Quadratic triangle elements with four Gauss points per element. The initial total DOFs to mesh this part was 1882.

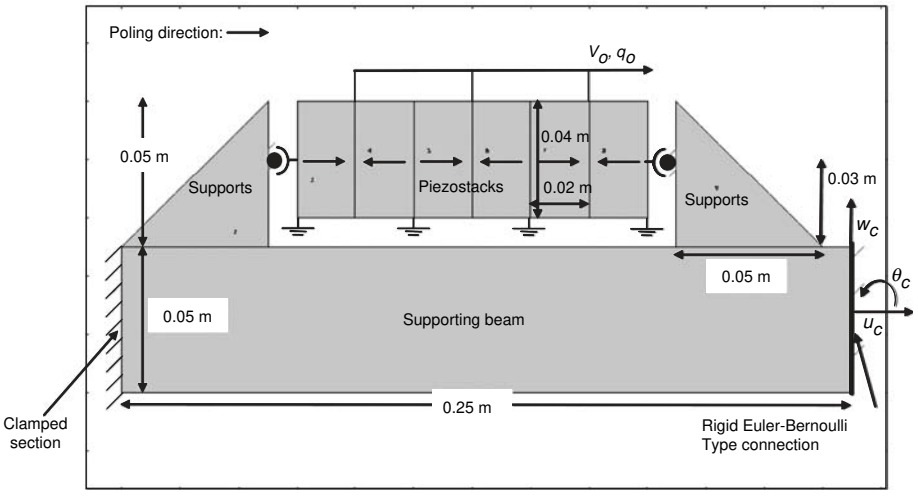

Figure 4. *Details of active substructure 1.*

Table 2. Piezostack characteristics.

Piezoelectric material		
Name	**Values**	**Mechanical properties**
$c11_E = c22_E$	1.27×10^{11} Pa	11 and 22 stiffness matrix coefficients
$c12_E$	8.02×10^{10} Pa	12 stiffness matrix coefficient
$c13_E = c23_E$	8.46×10^{10} Pa	13 and 23 stiffness matrix coefficients
$c33_E$	1.17×10^{11} Pa	33 stiffness matrix coefficient
$c44_E = c55_E$	2.30×10^{10} Pa	44 and 55 stiffness matrix coefficients
$c66_E$	2.34×10^{10} Pa	66 stiffness matrix coefficient
$e31 = e32$	6.62 Cm^{-2}	31 and 32 piezoelectric matrix coefficients
$e33$	-23.24 Cm^{-2}	33 piezoelectric matrix coefficient
$e24 = e15$	-17.03 Cm^{-2}	24 and 15 piezoelectric matrix coefficients
ρ	7500 kgm^{-3}	Density
$\varepsilon 33_S$	143.361 ε_o $CV^{-1}m^{-1}$	Dielectric permittivity
$\varepsilon 11_S = \varepsilon 22_S$	1704 ε_o $CV^{-1}m^{-1}$	Dielectric permittivity
n	6	Number of layers
ep	0.02 m	Layer thickness
la_p	0.01 m	Layer width
l_p	0.04 m	Layer height

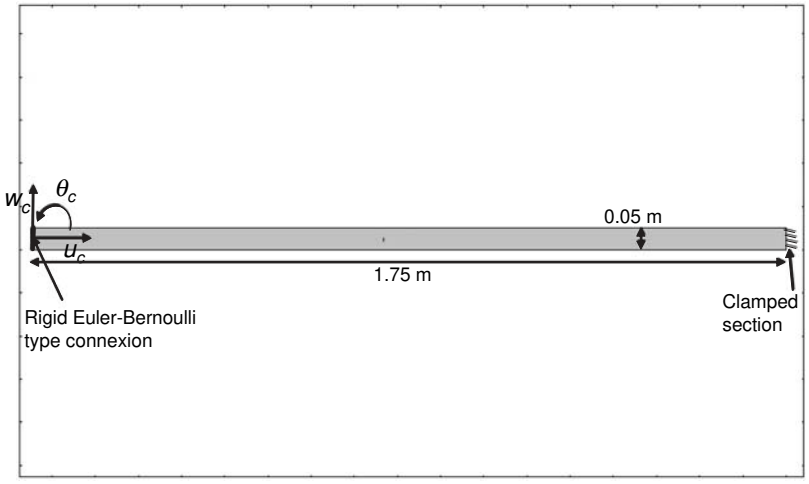

Figure 5. *The passive substructure 2.*

Implementation of Proposed Condensation

THE ACTIVE SUPER ELEMENT

The active substructure described above is condensed using the method proposed in section 'Linear Piezoelectric Mechanical Systems Modeling and Condensation'. We also build a super element with 3 static fields corresponding to the connecting 'Euler Bernoulli' type master DOFs as the solutions of Equation (18), one piezoelectric dual field as the solution of Equation (19) and five internal modes solutions of Equation (20). The static electrical field used for writing the piezoelectric dual constraint in Equations (18–20) is shown on Figure 6. Figures 7–9 show the first three displacement fields related to the static connecting master DOFs, Figure 10 the dual displacement field and Figures 11–13 the five internal modes. The eigenfrequencies of these internal modes are in Table 3. In the following numerical results, we consider three different mesh refinements of this active substructure. The meshing quality does not impact the size of the resulting super element but only the accuracy of the condensation procedure. In consequence, the total number of DOFs for the active super element is always nine.

THE PASSIVE SUPER ELEMENT

The passive super element is directly obtained by using a Craig and Bampton condensation technique. The element has three static master DOFs corresponding to the imposed connective 'Bernoulli Euler' displacement fields and 20 internal modes. The corresponding eigenfrequencies are compiled in Table 4.

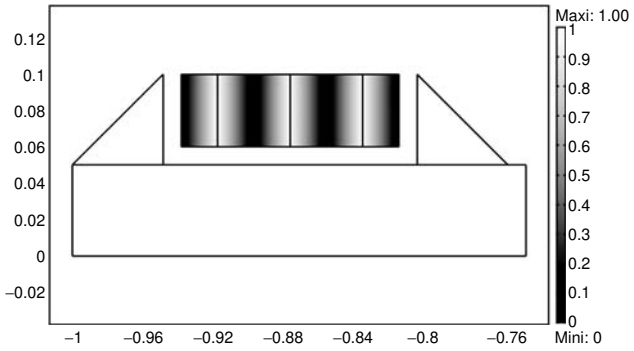

Figure 6. *Static imposed electrical field.*

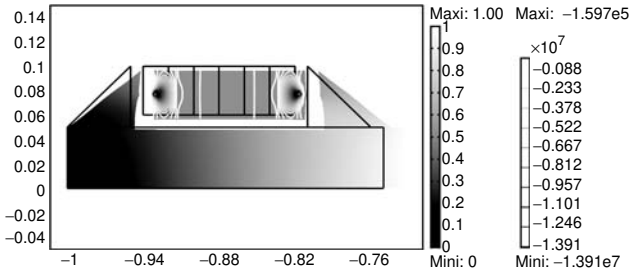

Figure 7. *Displacement norm and electrical fields of the first static connecting degree of freedom u_i^o.*

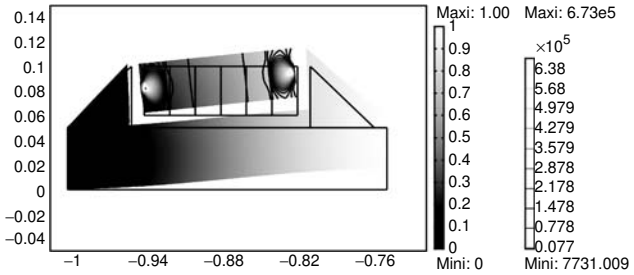

Figure 8. *Displacement norm and electrical fields of the second static connecting degree of freedom w_i^o.*

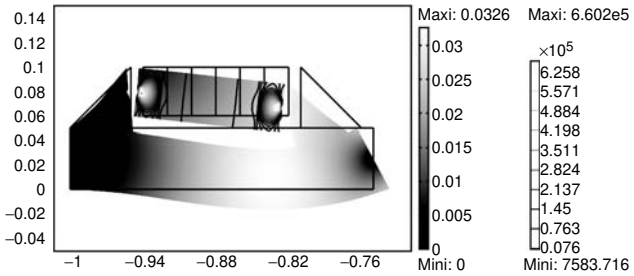

Figure 9. *Displacement norm and electrical fields of the third static connecting degree of freedom θ_i^o.*

Note that :

- According to Craig and Bampton assumptions (Geradin, 1997), the super element's frequency domain of validity extends to about 3800 Hz considering a criterion of one-half of the largest internal eigenfrequency.
- Therefore, the frequency range for the passive super element is less than that of the piezoelectric super element, 4200 Hz.

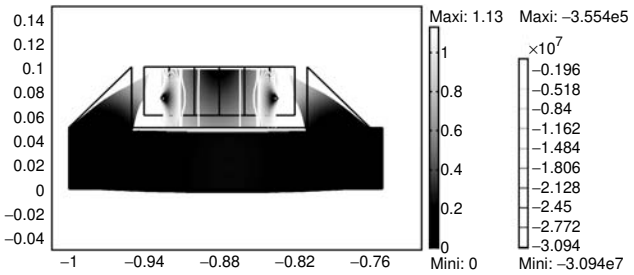

Figure 10. *Displacement norm and electrical fields of the piezoelectric dual stress field.*

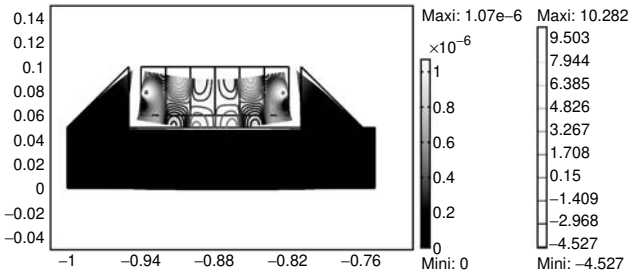

Figure 11. *Displacement norm and electrical fields of the first internal mode.*

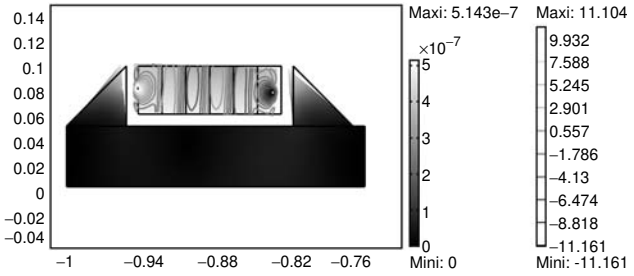

Figure 12. *Displacement norm and electrical fields of the second internal mode.*

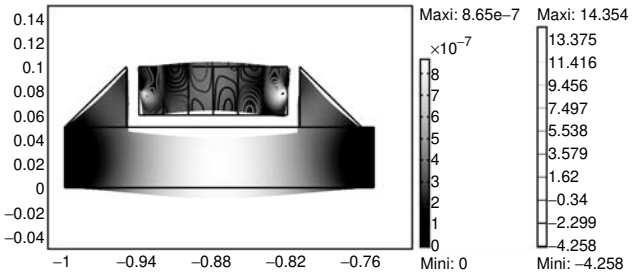

Figure 13. *Displacement norm and electrical fields of the third internal mode.*

Numerical Comparison Between Active Super Element Approach and Direct Modeling

To study the numerical efficiency of the proposed substructuring approach, a global model (GM) is also implemented. The meshed piezomechanical structure is depicted in Figure 14. It has 376 Lagrange Quadratic elements and 17509 DOFs. The model quality is also very good for this refined mesh system and exceeds that of each of the nominal substructures.

Table 3. Active super element internal eigenfrequencies.

Mode	Frequency (Hz)
1	2421
2	2968
3	3855
4	5642
5	8474

Table 4. Passive super element internal eigenfrequencies.

Mode	Frequency (Hz)	Mode	Frequency (Hz)
1	89.4	11	3151
2	244.5	12	3766
3	474.4	13	4416
4	774.3	14	4589
5	1139	15	5098
6	1531	16	5808
7	1565	17	6116
8	2046	18	6543
9	2576	19	7300
10	3061	20	7639

This GM system has the same mechanical and electrical boundary conditions as those presented above for each substructure. Even the 'Bernoulli-Euler' linking conditions is imposed so as to focus the analysis on the piezoelectric behavior and not on the validity of such an assumption. The applied electrical conditions could be either potential (Dirichlet conditions) or charge (Neumann conditions) on the driven electrode depending on which kind of problem we want to solve.

STATIC RESULTS

The static results are very important in these kinds of problem because they are linked in a large part to the piezoelectric behavior of the transducer as mentioned in section 'Linear Piezoelectric Mechanical Systems Modeling and Condensation':

- The ratios q_p/V_p and $\max(|w|)/V_p$ are directly connected to the static piezoelectric coupling effect.
- The difference between the ratios above and the dual ratios V_p/q_p and $\max(|w|)/q_p$ are directly connected to the induced stiffness modifications when the piezoelectric material acts under imposed voltage or imposed charge.

The static deformations and electric fields of the global meshed system and the substructured system under a unit imposed voltage $V_p = 1$ are presented in Figures 15 and 16. The obtained deformation and electrical fields appear identical in both pictures.

In order to assess the convergence quality of our approach, consider three different mesh refinements. The first case corresponds to the initial mesh (IM) defined above, labeled here as refined mesh 1 (RM 1). The second case, 'refined mesh 2' (RM 2), is an increased quality mesh for the active substructure with

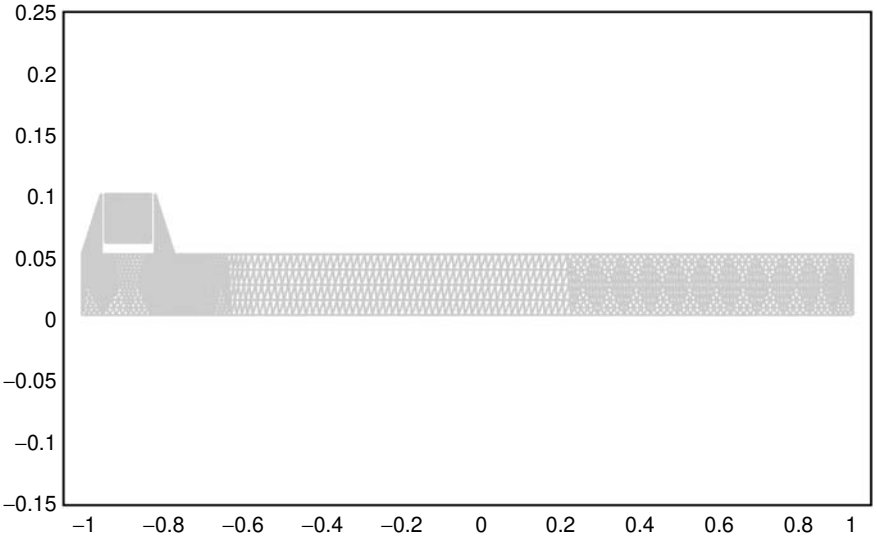

Figure 14. *The global meshed system.*

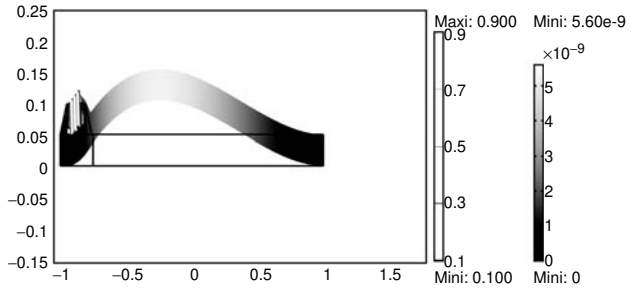

Figure 15. *Static displacement norm and electrical fields of the global meshed system under unit imposed voltage.*

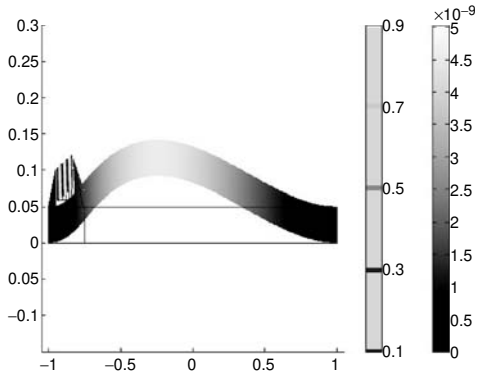

Figure 16. *Static displacement norm and electrical fields of the substructured system under unit imposed voltage.*

3256 elements and 20,490 DOFs. The third case, 'refined mesh 3' (RM 3), enhances the mesh refinement of the passive substructure with 840 elements and 3778 DOFs while also using the RM 2 for the active part. We re-emphasize that the condensed super elements have fixed numbers of DOFs. Table 5 presents the qualitative results for the system under a unit applied voltage. Table 6 shows the dual result obtained for the system under a unit applied charge. Figures 17 and 18 show the displacement norm and voltage fields of the deformed structures respectively obtained with the global and the substructured mesh.

The results obtained using the proposed substructured approach are very close to those obtained by a global mesh with a maximum error of 4%. As for the proposed method, in the formalism introduced here, imposed piezoelectric voltage as input and charge as output, the static response under unit applied voltage is much more precise with a maximum error of 2% on maximum displacement with the coarser mesh case than the static response for unit applied charge. Note that the models all yield the same value for the dielectric capacitance, C_p^o, since they use the same electrostatic representation. As shown in Table 6, the accuracy of the results increase with mesh refinement of the active subsystem. The results for the displacements, w, converge as $O(2)$ of the number of DOFs, while the voltage converges as $O(4)$.

Table 5. Static results comparison for different system meshes under unitary applied voltage.

Quantities	GM	IM (error)	RM 2 (error)	RM 3 (error)
q_p 10^{-9} C	1.54	1.54 (0%)	1.54 (0%)	1.54 (0%)
max($\|w\|$) 10^{-9} m	5.232	5.38 (2%)	5.25 (0.4%)	5.25 (0.4%)
C_p^o 10^{-10} $C \cdot V^{-1}$	1.5232	1.5232 (0%)	1.5232 (0%)	1.5232 (0%)

Table 6. Static results comparison for different system meshes under unitary applied voltage.

Quantities	GM	IM (error)	RM 2 (error)	RM 3 (error)
V_p 10^{+8} V	6.489	6.509 (3.1)	6.4916 (0.04%)	6.4915 (0.038%)
max($\|w\|$) m	3.395	3.49 (2.8%)	3.409 (0.4%)	3.409 (0.4%)
C_p^o 10^{-10} $C \cdot V^{-1}$	1.5232	1.5232 (0%)	1.5232 (0%)	1.5232 (0%)

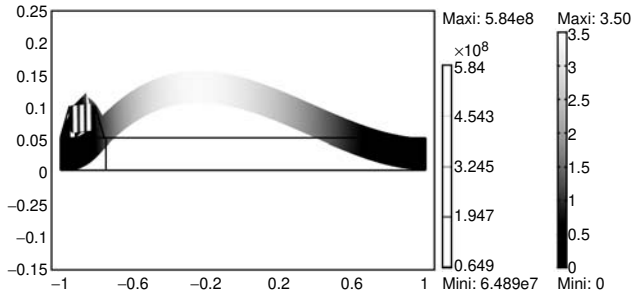

Figure 17. *Static displacement norm and electrical fields of the global meshed system under unitary imposed charge.*

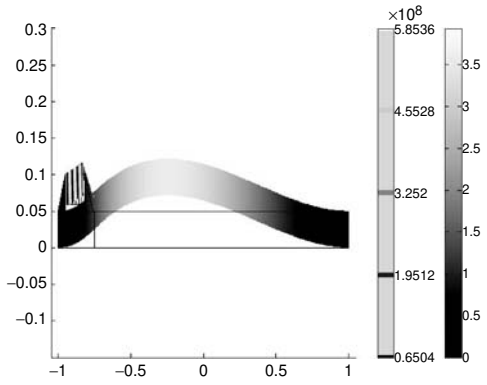

Figure 18. *Static displacement norm and electrical fields of the substructured system under unitary imposed charge.*

FREQUENCY RESPONSE FUNCTION COMPUTATION

The main interest of the proposed method is the ability to compute the global piezoelectric response functions by taking into account the global behavior of such a system. To demonstrate this capability, Figure 19 depicts the frequency response function of the piezoelectric charge for a unit voltage input, $q_p(\omega)/V_p(\omega)$.

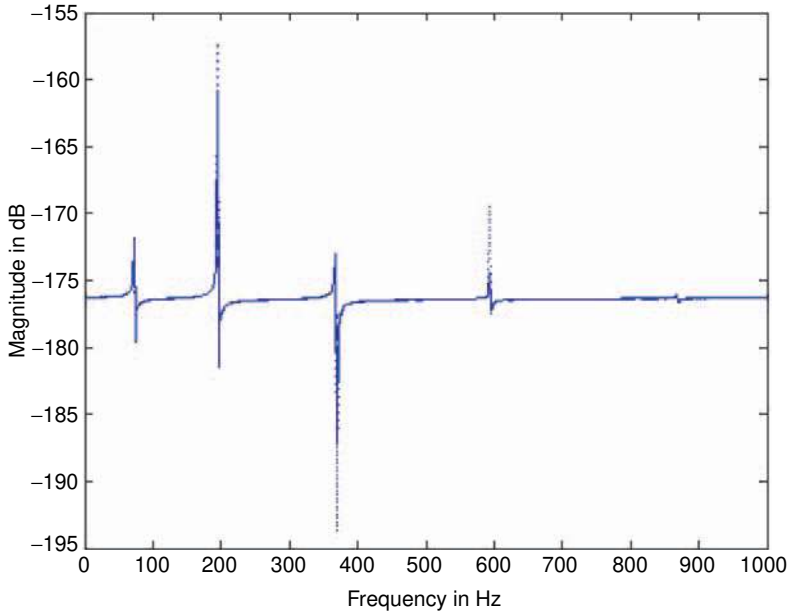

Figure 19. *FRF $q_p(\omega)/V_p(\omega)$ for the global mesh (dotted line), refined mesh 1 (dash line), 2 (dashdot line) and 3 (plain line).*

Table 7. The five first poles of the transfer function $q_p(\omega)/V_p(\omega)$.

Pole Number	GM	IM (error)	RM 2 (error)	RM 3 (error)
1	72.56 Hz	72.69 Hz (0.1%)	72.59 Hz (0.041%)	72.57 Hz (0.014%)
2	194.08 Hz	194.33 Hz (0.13%)	194.14 Hz (0.031%)	194.09 Hz (0.005%)
3	369.26 Hz	369.55 Hz (0.07%)	369.35 Hz (0.024%)	369.25 Hz (−0.003%)
4	594.17 Hz	594.52 Hz (0.059%)	594.38 Hz (0.035%)	594.15 Hz (−0.003%)
5	869.01 Hz	869.60 Hz (0.06%)	869.48 Hz (0.054%)	869.04 Hz (0.003%)

Table 8. The five first zeros of the transfer function $q_p(\omega)/V_p(\omega)$.

Zero Number	GM	IM (error)	RM 2 (error)	RM 3 (error)
1	72.95 Hz	73.10 Hz (0.2%)	72.98 Hz (0.041%)	72.967 Hz (0.023%)
2	194.78 Hz	195.06 Hz (0.14%)	194.83 Hz (0.026%)	194.79 Hz (0.005%)
3	369.90 Hz	370.19 Hz (0.078%)	369.95 Hz (0.013%)	369.85 Hz (−0.013%)
4	594.38 Hz	594.67 Hz (0.049%)	594.53 Hz (0.025%)	594.30 Hz (−0.013%)
5	869.02 Hz	869.64 Hz (0.071%)	869.53 Hz (0.059%)	869.09 Hz (0.008%)

Results for the four cases introduced in the previous section are shown: the global mesh, and refined mesh 1, 2, and 3. The figure does not reveal any 'visual' difference between the results. We note the well known closed poles/zeros location of the electric transfer function for a piezoelectric system. The distance between each successive pole and zero are closely related to the mechanical damping capability of the passively shunted circuit (Preumont, 1997; Monnier, 2005). These spacings can be enhanced by increasing the piezoelectric coupling coefficient but also by optimizing the mechanical coupling with a suitable approach as mentioned in (Monnier, 2005). Thus, the capability to compute these quantities are fundamental for optimizing active or passive control systems that use such a piezoelectric transducer.

The five first poles (resonance frequencies) and zeros (antiresonance frequencies) of the electrical transfer function $q_p(\omega)/V_p(\omega)$ are presented in Tables 7 and 8. Notice that the substructuring approach results are precise enough to compute poles and zeros location with a maximum error, here, of ~ 0.2 % with the initial mesh. The convergence of the method is clearly indicated by this set of numerical tests. Nevertheless, for the four cases, the refined mesh three yields some smaller frequencies than those of the reference global computation. These may come from specific error introduced by the two different numerical algorithms used here.

Finally, note that the differences between each successive electrical pole and zeros are not improved by the mesh refinement, it only increases the frequency resolution for each pole/zero pair.

MODAL SYNTHESIS OF A SEMI DISTRIBUTED PIEZOCOMPOSITE PLATE

Now consider the direct application of the proposed technique to the modal synthesis of a piezoelectric impedance dedicated LTI model. The aim is also to provide a reduced order LTI of a piezoelectric system capable to accurately compute impedances such as q_p/V_p but also electromechanical effects such as $q_p, V_p/F, w/V_p, q_p$ or mechanical impedance, w/F. The resulting simple model could also be used in optimization processes that employ numerous iterations.

Numerical Model

PIEZOMECHANICAL DESCRIPTION

The system, depicted in Figure 20, corresponds to that used by Hagood and von Flotow (Hagood, 1991). It is a cantilever beam on which are glued two pairs of piezoelectric patches. Each pair of patches can be considered as either actuator or sensor. The material properties are detailed in Tables 9 and 10 while the dimensions are in Figure 20. Each patch on each side of the beam has the same polarization direction through their thickness. The complete piezoelectric material characterization was not precisely found into literature. So, some values have been estimated by using different articles such as (Hagood, 1991; Shah and Joshi, 1993; Crawley, 1994). Inconsistencies between these articles for the same material, and inadequate specificity as to how the values were determined, lead us to simplify our estimation and assume the use of an isotropic mechanical behavior and permittivity tensor as previously employed in (Crawley, 1994).

Table 9. Beam characteristics.

Structural material		
Name	**Values**	**Mechanical properties**
E	6.3×10^{10} Pa	Young's Modulus
ν	0.30	Poisson Ratio
ρ	2700 kgm^{-3}	Density

Table 10. Piezostack characteristics.

Piezoelectric material		
Name	**Values**	**Mechanical properties**
$s11_E = s22_E = s33_E$	15.9×10^{-12} Pa^{-1}	11, 22, and 33 compliance matrix coefficients
$s12_E = s13_E = s23_E$	-4.13×10^{-12} Pa^{-1}	12, 13, and 23 compliance matrix coefficient
$s44_E = s55_E = s66_E$	41.3×10^{-12} Pa^{-1}	44, 55, and 66 compliance matrix coefficients
$d31 = d32$	-254×10^{-12} CN^{-1}	31 and 32 piezoelectric matrix coefficients
$d33$	580×10^{-12} CN^{-1}	33 piezoelectric matrix coefficient
$d24 = d15$	730×10^{-12} CN^{-1}	24 and 15 piezoelectric matrix coefficients
ρ	7600 kgm^{-3}	Density
$\varepsilon33_T = \varepsilon11_T = \varepsilon22_T$	2780 ε_o $CV^{-1}m^{-1}$	Dielectric permittivity

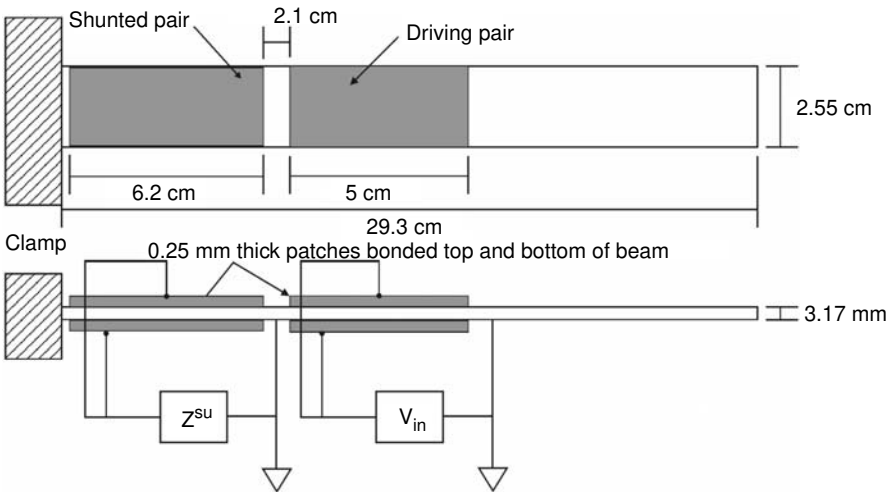

Figure 20. *The considered piezoelectric beam system.*

The electrical boundary conditions applied to each patch are:

- Lateral faces are free of charge.
- Face in contact with the beam is grounded.
- Controlling voltage is applied on the external face, $V_{1,2}$, where the subscript 1 indicates the pair located near the clamped edge and 2 for the other pair. The dual charge is $q_{1,2}$.

To assess the capability of the super element synthesis to address mechanical quantities, an external force F is applied in the middle of the free edge of the beam. The collocated displacement w_F is also computed. The LTI representation of such a system has three inputs: V_1, V_2, F, and three outputs: q_1, q_2, and w_F.

STUDIED MESH CASES

The system is meshed using Lagrange-Quadratic quadrangular elements with four Gauss points per element. This 3D element was chosen to emphasize the generic capability of such an approach even in the case of thin-layer modeling. By using this generic approach, even if it is not particularly adapted to thin composite layer modeling, we avoid modeling issues pertaining to the choice of a composite beam or plate model. Two different refined mesh cases are taken into consideration as depicted in Figures 21 and 22. In each case we use two elements in the thickness for each piezoelectric layer.

Mesh case 1 has 34,371 DOFs in 896 elements. Refined mesh case 2 has 70,213 DOFs in 1896 elements.

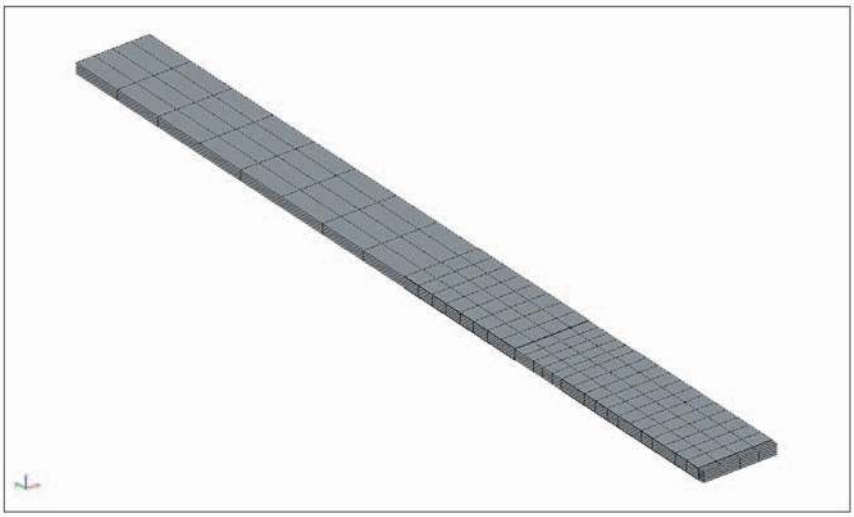

Figure 21. *Mesh case 1.*

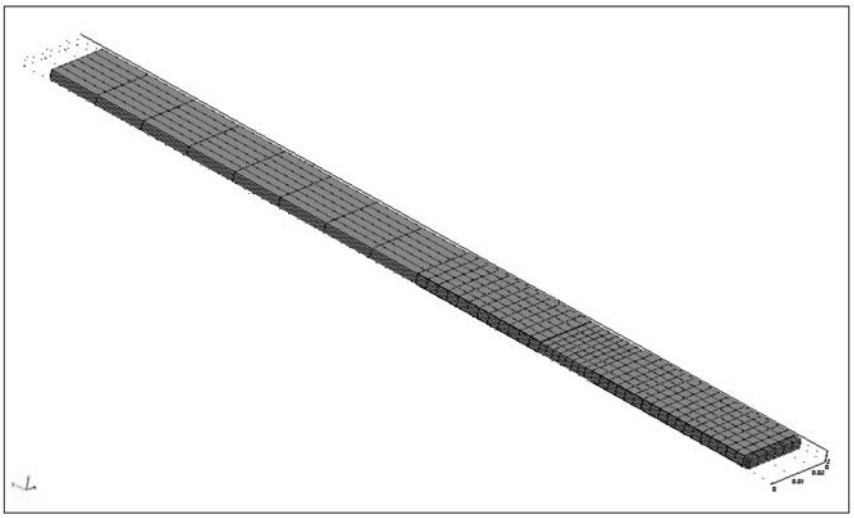

Figure 22. *Refined mesh case 2.*

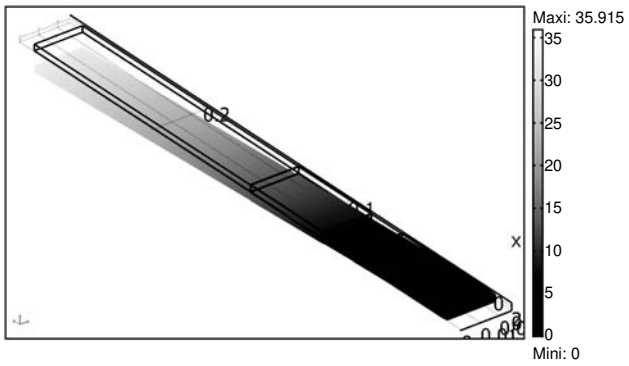

Figure 23. *First dual piezo stress field. Isosurfaces: Piezo voltage [V]; Displacement [m].*

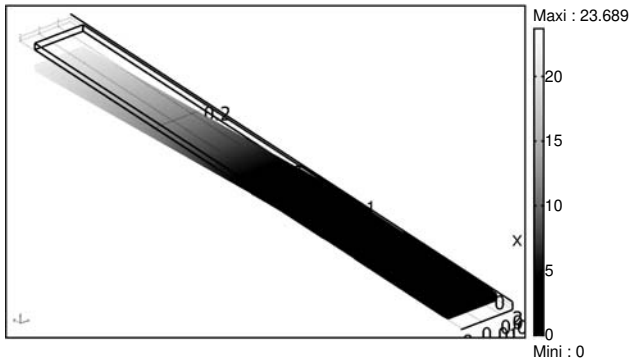

Figure 24. *Second dual piezo stress field. Isosurfaces: Piezo voltage [V]; Displacement [m].*

MODIFIED MODAL SYNTHESIS METHOD

The modal synthesis is performed by applying the proposed approach without computing any linking displacement fields. We only compute two sets of approximation fields corresponding to the solution of Equations (19) and (20). The complete behavior of the piezoelectric system is also projected on the results. The system is condensed by using the so-called modified modal synthesis method which adds the piezoelectric dual field stress to the classical modal approach.

The two specific fields corresponding to the solutions for each piezopatch of Equation (19) are shown in Figures 23 and 24.

Table 11 presents for the two mesh cases the first 20 frequencies of the inner modes as solution of Equation (20). It is apparent that the refined mesh case 2 does not induce a significant accuracy improvement in the frequency computation, with a maximum variation of about 0.4% in the estimate for the 12th mode.

The electrostatic equivalent capacitances of each pair of patches are obtained respectively equal to $C_1^o = 1.92e-7\ CV^{-1}$ and $C_2^o = 1.55e-7\ CV^{-1}$ in both mesh cases.

Table 11. Internal eigenfrequencies (in Hz) of the passive super element.

Mode	MC 1	MC 2	Mode	MC 1	MC2
1	37.61	37.58	11	3353.8	3340.5
2	203.30	203.20	12	3781.7	3781.0
3	256.75	256.71	13	3812.3	3808.9
4	553.40	553.10	14	4329.3	4328.9
5	705.14	702.30	15	4439.7	4422.0
6	1067.1	1066.6	16	5064.1	5058.4
7	1430.7	1430.5	17	5969.2	5945.7
8	1824.2	1823.0	18	6582.6	6573.7
9	1876.7	1869.2	19	6883.2	6881.6
10	2679.9	2677.8	20	7551.7	7522.9

Static Numerical Results

As our LTI model has three inputs and three outputs, there are a maximum of 27 possible charge cases if we want to explore all primal and dual solutions; this number of cases cannot be concisely presented. Instead, consider the first piezoelectric patch as the only actuator on which can be applied either voltage or charge with Dirichlet or Neumann boundary conditions imposed on the second piezoelectric patch. The external applied force is also considered as the only mechanical perturbation. This reduces the space such that only eight cases are computed. Tables 12 and 13 contain the results.

Table 12 clearly indicates that the two piezoelectric patches are electrically quasi-uncoupled. Increasing the number of modes used does not improve the numerical computation whereas the refinement enhances the voltage approximation as well as for electrical (Table 12) and mechanical perturbations (Table 13). The proposed modal synthesis method enables one to obtain very accurate static results compared to those given by a nonsubstructured global computation. Further, note that the charge estimation is almost the same between the cases. Finally, the computed voltage exhibits a maximum error of about 1.9% compared to the global mesh.

Dynamic Results and Electric Impedance Computation

As was done in the first example, Table 14 presents the first three flexural pole-zero estimates for the different cases. Note that increasing the number of modes does not improve the computed results. The proposed synthesis method introduces a maximum bias of 0.16% on the estimation of the electrical poles/zeros. This is due to the numerical procedure used to solve the constrained problems. The numerical procedure is improved by mesh refinement and demonstrates the convergence property of such approaches. These computations indicate a very close location between poles and zeros. The differences depend on the piezomechanical coupling

Table 12. Static results for different electrical applied conditions and different modeling approaches and mesh refinements: modal synthesis with 10 or 20 modes, global mesh. (EBC stands for 'electrical boundary conditions', MC for 'mesh case').

P1 EBC	P2 EBC	Quantities	MC 1 10 modes	MC2: 10 modes	MC 1: 20 modes	MC 2: 20 modes	MC1 Glob Mesh	MC2 Glob Mesh
	$q_2=0$	q_1 (μC)	0.262	0.263	0.262	0.263	0.265	0.265
		V_2 (mV)	−0.234	−0.225	−0.234	−0.225	−0.236	−0.227
$V_1=1$		w_F (μm)	−2.30	−2.30	−2.30	−2.30	−2.28	−2.28
	$V_2=0$	q_1 (μC)	0.262	0.263	0.263	0.263	0.265	0.265
		q_2 (pC)	49.7	47.7e	49.7	47.6	50.6	48.6
		w_F (μm)	−2.30	−2.30	−2.30	−2.30	−2.28	−2.28
	$q_2=0$	V_1 (MV)	3.81	3.81	3.81	3.81	3.76	3.77
		V_2 (kV)	−0.893	−0.855	−0.894	−0.855	−0.893	−0.856
$q_1=1$		w_F (m)	−8.78	−8.75	−8.78	−8.75	−8.63	−8.59
	$V_2=0$	V_1 (MV)	3.81	3.81	3.81	3.81	3.78	3.77
		q_2 (mC)	0.189	0.181	0.189	0.181	0.191	0.183
		w_F (m)	−8.78	−8.75	−8.78	−8.75	−8.62	−8.59

Table 13. Static results for a unitary applied force F and different modeling approaches and mesh refinements: modal synthesis with 10 or 20 modes, global mesh. (EBC stands for 'electrical boundary conditions', MC for 'mesh case').

P1 EBC	P2 EBC	Quantities	MC 1 10 modes	MC2: 10 modes	MC 1: 20 modes	MC 2: 20 modes	MC1 Glob Mesh	MC2 Glob Mesh
	$q_2=0$	q_1 (μC)	−2.30	−2.30	−2.30	−2.30	−2.28	−2.28
		V_2 (V)	5.80	5.79	5.80	5.79	5.72	5.71
$V_1=0$		w_F (mm)	1.32	1.32	1.32	1.32	1.33	1.33
	$V_2=0$	q_1 (μC)	−2.30	−2.30	−2.30	−2.30	−2.28	−2.28
		q_2 (μC)	−1.23	−1.23	−1.23	−1.22	−1.22	−1.22
		w_F (mm)	1.33	1.3	1.33	1.33	1.33	1.34
	$q_2=0$	V_1 (V)	8.78	8.75	8.78	8.75	8.62	8.59
		V_2 (V)	5.80	5.79	5.80	5.79	5.71	5.70
$q_1=0$		w_F (mm)	1.30	1.30	1.30	1.30	1.31	1.31
	$V_2=0$	V_1 (V)	8.78	8.75	8.78	8.75	8.62	8.59
		q_2 (μC)	−1.23	−1.23	−1.23	−1.23	−1.22	−1.22
		w_F (mm)	1.31	1.31	1.31	1.31	1.32	1.32

Table 14. Poles/Zeros evaluations (Hz) for different modeling approaches and mesh refinements: modal synthesis with 10 or 20 modes, global mesh. (EBC stands for 'electrical boundary conditions', MC for 'mesh case').

P2 EBC	q_1/V_1	Number	MC 1 10 modes	MC2: 10 modes	MC 1: 20 modes	MC 2: 20 modes	MC1 Glob mesh	MC2 Glob mesh
	Poles	1	35.917	35.900	35.917	35.900	35.872	35.860
		2	198.70	198.64	198.70	198.64	198.44	198.39
$V_2=0$		3	546.70	546.47	546.70	546.47	545.84	545.63
	Zeros	1	36.267	36.252	36.267	36.252	36.211	36.196
		2	199.41	199.35	199.41	199.35	199.12	199.06
		3	547.00	546.77	547.00	546.77	546.12	545.90
	Poles	1	35.997	35.983	35.997	35.983	35.950	35.937
		2	199.19	199.13	199.19	199.13	198.92	198.86
$q_2=0$		3	548.12	547.89	548.12	547.89	547.22	547.00
	Zeros	1	36.349	36.333	36.349	36.333	36.291	36.276
		2	199.89	199.82	199.89	199.82	199.59	199.52
		3	548.42	548.18	548.42	548.18	547.50	547.27

coefficient, therefore, on the mechanical design and on the piezoelectric coupling coefficient k_{31}. To optimize the use of such devices for active or passive applications requires good numerical accuracy in poles/zeros computation as underlined in (Preumont, 1997; Monnier, 2005). The possibility to reach a good compromise between numerical complexity and precision makes our method very attractive to be used in such procedures.

Table 15 presents the computed zeros for the mechanical transfer function. Obviously, the poles

Table 15. First three nonnull zeros (in Hz) of the mechanical transfer function w_F/F for different modeling approaches and mesh refinements: modal synthesis with 10 or 20 modes, global mesh. (EBC stands for 'electrical boundary conditions', MC for 'mesh case').

P1 EBC	P2 EBC	Number	MC 1 10 modes	MC2: 10 modes	MC 1: 20 modes	MC 2: 20 modes	MC1 Glob mesh	MC2 Glob mesh
	$V_2 = 0$	1	139.83	139.79	139.75	139.71	139.55	139.51
		2	256.75	256.71	256.75	256.71	256.68	256.64
$V_1 = 0$		3	445.94	445.77	445.00	444.83	444.20	444.04
	$q_2 = 0$	1	139.95	139.91	139.86	139.82	139.67	139.62
		2	256.75	256.71	256.75	256.71	256.68	256.64
		3	447.56	447.38	446.62	446.44	445.78	445.61

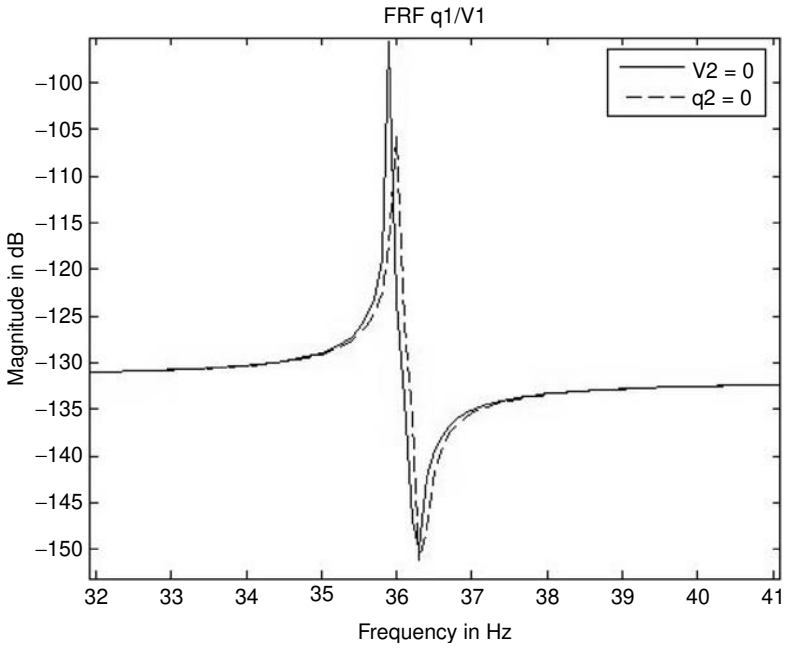

Figure 25. *Frequency response function q_1/V_1 for $q_2 = 0$ and $V_2 = 0$.*

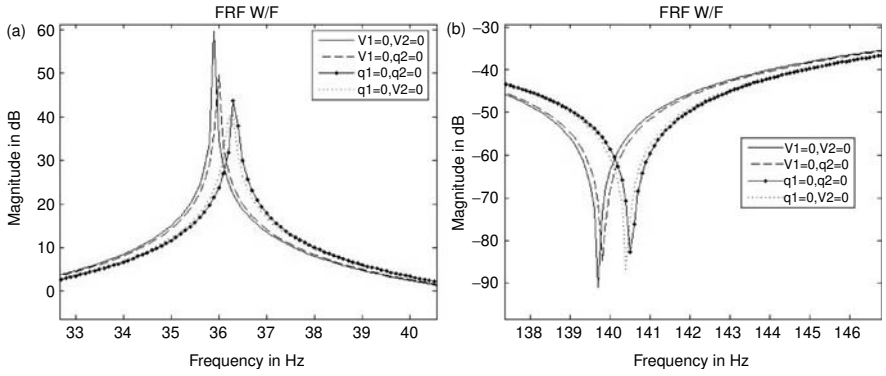

Figure 26. *Frequency response function w_F/F for any kind of electrical boundary conditions.*

correspond to those presented in Table 14. We clearly observe the influence of the number of modes on the numerical accuracy of the mechanical transfer function. As previously mentioned, the proposed synthesis method introduces a maximum numerical error of 0.14%. Once again, the condensation method allows one to obtain an accurate estimation of the mechanical behavior while using fewer DOFs.

Finally, we present in Figures 25 and 26 and the frequency response functions corresponding to unit

applied voltage on the first piezoelectric patch and to unit applied force F, for the refined condensed model with 20 inner modes. The difference between the locations of the poles and zeros for these cases is due to the electrical connection. These small perturbations are of great importance for patch impedance optimization for control of beam response. The proposed piezoelectric modal synthesis allows one to accurately introduce the underlying coupling phenomena in the suitable condensed model for optimization-intensive procedures.

CONCLUDING REMARKS

We have presented here an original numerical approach to build a condensed super element for a piezo-mechanical sub-system. The proposed method allows accurate modeling of the specific piezoelectric coupling phenomena. Thus, the reduced order model is able to precisely evaluate any kind of electrical, mechanical, or mixed transfer function. Attention has been paid in the analysis to the numerical accuracy in computing the static response and therefore the location of the zeros of the input/output system. As these quantities are important for passive or active optimization of such a piezoelectric transducer, the procedure provides a suitable and accurate condensed model able to be intensively used in numerical procedures.

The proposed methodology corresponds to a modified Craig and Bampton condensation able to take into account the entire piezoelectric coupling as far as it is accurately introduced in the basic model employed. This work showed characteristic results for two examples using '2D plane constrained' and complete '3D' models. The method could be applied for any piezoelectric approach as far as the electrical inputs/outputs are well defined in the approach.

Consideration of the convergence properties for the approach indicate that the precision in the electrical input/output transfer functions depend on the mesh refinement of the basic model and does not depend on the number of internal modes used in the super element. The mechanical and mixed transfer functions also converge like for the Craig and Bampton approach, depending on the mesh refinement and on the introduced modes.

Finally, note that the proposed approach allows one to achieve complete multiphysics models including complex piezoelectric mechanical and acoustical parts coupled with models of attached electronics. The method should permit one to address the problem of the complete optimization of electrical circuits for passive/active control or energy harvesting using piezoelectric transducers.

ACKNOWLEDGEMENTS

This work was carried out thanks to the exchanges induced and supported by the International Joint Research Unit: UMI2958 Georgia Tech-CNRS. Thus, we gratefully acknowledge Georgia Tech and the French CNRS for allowing such international collaborations.

REFERENCES

Allik, H.T.H. 1970. "Finite Element Method for Piezoelectric Vibration," *Int. J. Num. Methods Engrg*., 2(2):151–157.

Allik, H.K.M. and Webman, J.H. 1974. "Vibrational Response of Sonar Transducers using Piezoelectric Finite Elements," *J. Acoust. Soc. Am*., 56(6):1782–1791.

Banks, H.R.C. and Smith, Y.W. 1996. "*Smart Material Structures Modeling Estimation and Control*," Masson and Wiley.

Becker, J.O. and Fein, M.M.L.G. 2006. "Finite Element-based Analysis of Shunted Piezoelectric Structures for Vibration Damping," *Computers and Structures*, 84(31–32):2340–2350.

Benjeddou, A. 2000. "Advances in Piezoelectric Finite Element Modeling of Adaptive Structural Elements: A Survey," *Computers and Structures*, 76(1–3):347–363.

Bernadou, M.C.H. 2003. "Modelisation and Numerical Approximation of Piezoelectric thin Shell. Part II : Approximation by Finite Element Methods and Numerical Experiments," *Comput. Method. Appl. Mech. Engrg*., 192(37–38):4045–4073.

Carrera, E. 1997. "An Improved Reissner-Mindlin Type Model for the Electro-Mechanical Analysis of Multilayered Plates Including Piezo-Layers," *J. Intell. Mat. Syst. Struct*., 8(3):496–508.

Chattopadhyay, A.C.S. 1997. "A Higher Order Theory for Modeling Composite Laminates with Induced Strain Actuators," *Composites Part B*, 28(3):243–252.

Collet, M.L.J. 1995. "Active Control with Piezoelectric Layers Optimization," *Journal of Structural Control*, 1:59–79.

Collet, M. 2001. "Shape Optimization of Piezoelectric Sensors Dealing with Spill-Over Instabilities," *IEEE Transactions on Control System Technology* 9(4):654–663.

Collet, M.V. and Walter, P.D. 2003. "Active Damping of a Micro-Cantilever Piezo-Composite Beam," *Journal of Sound and Vibration*, 260(3):453–476.

Collet, M.P. and Delobelle, V.W. 2004. "Active Damping with Piezoekectric MEMS Devices," *Smart Structures and Material Conf (Active Damping)*, SPIE, pp. 301–309.

Crawley, E. 1994. "Intelligent Structures for Aerospace: A Technology Overview and Assessment," *AIAA Journal*, 32(8):1689–1699.

Fernadez, A.J.P. 2004. "Analytical and Numerical Modelling of Laminated Composites with Piezoelectric Elements," *Journal of Intl. Mat. Syst. and Struc*., 15(9–10):753–761.

Geradin, M.D.R. 1997. "Mechanical Vibrations: Theory and Applications to Structural Dynamics," *J. Wiley and Sons*.

Ha, S. 1990. "Finite Element Analysis of Sandwich Plates: An Overview," *Comp Struc*., 37(1):1–21.

Hac, A.L.L. 1993. "Sensor and Actuator Location in Motion Control of Flexible Structures," *Journal of Sound and Vibration*, 167(2):239–261.

Hagood, N.W.A.H.v.F. 1991. "Damping of Structural Vibrations with Piezoelectric Materials and Passive Electrical Networks," *Journal of Sound and Vibration*, 146(2):243–268.

Kogl, M.M.B. 2005. "Analysis of Smart Laminates using Piezoelectric Mitc Plate and Shell Elements," *Computers and Structures*, 83(15–16): 1153–1163.

Lee, C.K.F.M. 1989a. "Laminated Piezopolymer Plates for Torsion and Bending Sensors and Actuators," *J. Acoust. Soc. Am*, 87(3):2432–2439.

Lee, C.K.F.M. 1989b. "Laminated Piezopolymer Plates for Torsion and Bending Sensors and Actuators," *J. Acoust. Soc. Am*, 87(3):2432–2439.

Lee, C. 1990. "Theory of Laminated Piezoelectric Plates for the Design of Distributed Sensors/Actuators. Parts III," *J. Acoust. Soc. Am.*, 87(3):1144–1157.

Lee, C.-K., Chiang, W.-W. and O'Sullivan, T.C. 1991. "Piezoelectric Modal Sensor/Actuator Pairs for Critical Active Damping Vibration Control," *Journal of Acoustical Society of America*, 90(1):374–384.

Lin, M.W.A.O. and Abatan, C.R. (1994). "Application of Commercial Finite Element Codes for the Analysis of Induced Strain-Actuated Structures," *J. Intell. Mater. Syst. Struct.*, 5(6):869–875.

Mackerle, J. 1997. "Finite Element Linear and Nonlinear Static and Dynamic Analysis of Structural Elements: A Bibliography (1992–1995)," *Engrg. Computations*, 14(4):347–440.

Maurini, C.F. and dell'Isola, J.P. 2004. "On Model of Layered Piezoelectric Beam for Passive Vibration Control," *Journal de Physique IV*, 115(1):307–316.

Monnier, P.M.C. 2005. "Definition of the Mechanical Design Parameters to Optimize Efficiency of Integraol Force Feedback Active Damping Strategy," *Journal Structural Control and Health Monitoring*, 12(1):65–89.

Meyer, Y.T. and Verdot, M.C.M. 2007. "Active Isolation of Electronic Micro-Components with Piezoelectrically Transduced Silicon Mems Devices," *J. Smart. Mat. and Struct.*, 16(1):128–134.

Noor, A. 1991. "Bibliography of Books and Monographs on Finite Element Technology," *Appl Mech Rev*, 44(1):307–317.

Preumont, A. 1997. *Vibration Control of Structures : An introduction*, Kluwer.

Rajapakse, R. (1997). Boundary element method for piezoelectric solids, *In Varadan VV, Chandra J editors. Smart Struct Mater Washington*, SPIE, pp. 418–427.

Rao, S.S.M.S.M. 1994. "Piezoelectricity and its Use in the Disturbance Sensing and Control of Flexible Structures: A Survey," *Appl. Mech. Rev.*, 47(4):113–123.

Rixen, D. J. 1998. "Dual Schur Complement Method for Semi-Definite Problems," *Contemporary Mathematics*, 218(1):341–348.

Saravanos, D.A.P.R. and Heyliger, D.H. 1997. "Layerwise Mechanics and Finite Element for the Dynamic Analysis of Piezoelectric Composite Plates," *Int. Jour. Solids. Struct.*, 34(3):359–378.

Shah, D.K.S.P. and Joshi, W. C. 1993. "Static Structural Response of Plates with Piezoceramic Layers," *Smart Materials and Structures*, 2:172–180.

Tzou, H.S.H.F. 1994a. "A Study of Segmentation of Distributed Piezoelectric Sensors and Actuators, Part I: Theorical Analysis," *Journal of Sound and Vibration*, 172(2):247–259.

Tzou, H.S.H.F. 1994b. "A Study of Segmentation of Distributed Piezoelectric Sensors and Actuators, Part II : Parametric Study and Active Vibration Controls," *Journal of Sound and Vibration*, 172(2):261–275.

Tzou, H. 1997. "*Vibration Control of Structures : An introduction*, Kluwer.

Varadan, V.V.Y.H. and Lim, V.V. 1996. "Closed Loop Finite-Element Modeling of Active/Passive Damping in Structural Vibration Control," *Smart Materials and Structures*, 5(5): 685–694.

Vidoli, S.F.D. 2001. "Vibration Control in Plates by Uniformly Distributed PZT Actuators Interconnectd via Electric Networks," *Eur. J. Mech. A/Solids* 20:435–456.

Wang, S. 2004. "A Finite Element Model for the Static and Dynamic Analysis of Piezoelectric Bimorph," *Int. Journal of Solid. and Structures*, 41(15):4075–4096.

Yang, H.T.Y.S. and Saigal, S.D.L. 1996. "Advances of Thin Shell Finite Elements and Some Applications Vers I," *Smart. Struct. Mat.*, 35(4):481–504.